Higher Order Boundary Elements: An Applicable Concept for Hydrodynamic Analysis?

Grant E. Hearn

Marine Technology Department, University of Newcastle upon Tyne,

Newcastle upon Tyne, NE1 7RU, UK

ABSTRACT

This paper considers the use of Higher Order Boundary Elements (HOBEs) with different zero speed and forward speed formulations of offshore related fluid-structure interactions for floating structures in open water conditions. The fluid is assumed inviscid and the flow is irrotational. Sample results of the application of the HOBE method in the prediction of second order forces are then presented for an offshore barge and a semi-submersible. In the latter case the theoretical predictions are compared with earlier predictions and independent experimental measurements. A discussion of the advantages and the special precautions to be observed when using the HOBE solution technique are highlighted.

1. INTRODUCTION

The terms boundary integral equation (B.I.E) and boundary element method (B.E.M) will be treated synonymously in this paper, since both formulations are based on the application of Green's second identity. It is only the choice of the kernel of the resulting integral equation which makes the two techniques differ. In the B.I.E approach the integral equation kernel, or Green function, automatically satisfies Laplace's equation and the boundary conditions on all surfaces, but the wetted surface of the floating structure. In the B.E.M the kernel is selected to be a solution of Laplace's equation and may or may not satisfy other boundary conditions depending upon the depth of the fluid. In either case it is quite normal to assume invariance of the unknown dependent variable of velocity potential or source strength over the elements used to discretise the bounding surface of the formulation. This assumption leads to discontinuous solutions.

In an earlier paper [1] 2D Green function based HOBEs were developed and applied to investigate the radiation and diffraction analysis of floating and submerged structures at zero forward speed. The term higher order boundary element simply indicates that the panels of the surface discretisation process are no longer flat and the behaviour of the selected dependent variable is given a higher order functional representation over the curved panels. This means that HOBE solutions are continuous across the panel boundaries. In this paper the concept of HOBEs is extended to include a number of different 3D formulations. The formulations are based on the Green function method and the concept of an inner-outer domain matching technique using either the Sommerfeld radiation condition or what we have called the Green Function Matching technique [2].

The paper is organised as follows. After presenting the different possible formulations for solving the first-order fluid-structure interaction problems, with and without forward speed influences included, the fundamental ideas and basic mathematical relationships of the HOBE approach are outlined. Without derivation the method of evaluating the second order forces is presented and then applied to provide estimates of the second order forces experienced by an offshore barge and a semi-submersible. Finally, some of the advantages and disadvantages of the various proposed HOBE formulations are discussed and conclusions presented.

2. HYDRODYNAMIC MODELS

The zero speed Green function integral equations may be expressed as either

$$-\alpha\phi + \int_{S_w} \phi \frac{\partial G}{\partial n} ds = \int_{S_w} G\, v_n ds, \tag{1}$$

with G corresponding to a pulsating source, or

$$\begin{aligned} -\alpha\phi + \int_{S_w} \phi \frac{\partial G}{\partial n} ds + \int_{S_r} \left[\phi \frac{\partial G}{\partial n} - G \frac{\partial \phi}{\partial n}\right] ds \\ + \int_{S_f} \left[\phi \frac{\partial G}{\partial n} - \frac{\omega^2}{g} \phi G\right] ds = \int_{S_w} G\, v_n ds \end{aligned} \tag{2}$$

where G, equal to $1/r$, is the simpler Rankine source with r equal to the distance between the fluid singularity location point and some generic point in the fluid. In either case n denotes an outward normal direction and v_n denotes the wetted surface radiation and diffraction boundary conditions applicable on the surface of the structure S_w. The outward normal direction on any surface is positive when pointing into the fluid. In the latter formulation $\frac{\partial \phi}{\partial n}$ is specified on the free-surface, S_f, using the linearised zero forward speed free-surface condition, but it still requires specification on the radiation boundary S_r. This may be achieved by direct application of the Sommerfeld radiation condition [3]

$$\frac{\partial \phi}{\partial R} = \left[im_0 - \frac{1}{2R}\right]\phi, \tag{3}$$

or through some matching technique, as implied by

$$\phi_{\Omega I} = \phi_{\Omega O} \text{ and } \left(\frac{\partial \phi}{\partial n}\right)_{\Omega I} = \left(\frac{\partial \phi}{\partial n}\right)_{\Omega O}, \tag{4}$$

where m_0 is the wavenumber determined from the dispersion equation and Ω^I and Ω^O denote the inner and outer fluid domains respectively. The outer domain solution may be provided by an eigenfunction expansion [3] or we may construct an artificial outer problem [3] in the fluid domain exterior to the radiation surface S_τ. Here S_τ is treated as a vertical cylindrical surface with a base. For example, S_τ might be an open rectangular box or a circular or elliptical cylindrical can. The artificial outer problem is then formulated using the conventional Green function formulation of Equation (1), which is now based on S_τ rather than S_w. Denoting the outer domain solution by ϕ' this formulation is 'solved' for $\frac{\partial \phi'}{\partial n}$ rather than ϕ'. Designated the Green Function Matching technique this approach treats the associated integral equation as first kind Fredholm, rather than second kind Fredholm, since it is used to provide $\frac{\partial \phi'}{\partial n}$ on S_τ. That is, we use

$$-\alpha\phi' + \int_{S_\tau} \phi' \frac{\partial G}{\partial n} ds = \int_{S_\tau} G \frac{\partial \phi'}{\partial n} ds, \qquad (5)$$

where the minus sign correctly takes into account the difference in sign of the outward normal on S_τ for the inner and outer problems. The reason for formulating such a procedure is that the outer solution may be formulated and stored once for any convenient shape of radiation boundary for each frequency. Thereafter only the inner problem changes as the geometry of the structure to be analysed changes and the outer formulation details are simply read back each time.

The forward speed problem may be considered from a number of different viewpoints. For low frequency damping calculations [4,5] the zero speed problem of Equation (1) may be used with the incident wave frequency ω replaced by the encounter wave frequency ω_e. This 'equivalent' zero speed problem is then solved using any one of the three methods described through Equations (1) to (5). Thereafter the effect of the forward speed is accounted for by application of the usual strip-theory form of corrections to the zero speed velocity potentials calculated[6]. Alternatively we may utilise the linearised forward speed Green function formulation

$$\begin{aligned} -\alpha\phi + \int_{S_w} \phi \frac{\partial G}{\partial n} ds - 2i\frac{U\omega_e}{g} \oint_{L_0} G\phi dy \\ + \frac{U^2}{g} \oint_{L_0} \left[\phi \frac{\partial G}{\partial x} - G\frac{\partial \phi}{\partial x}\right] dy = \int_{S_w} G\, v_n ds \end{aligned}, \qquad (6)$$

where G now corresponds to a translating pulsating source. This formulation assumes that the interaction between the wavemaking potentials and the unsteady wave interaction potentials are negligible. Since computation of the pulsating and translating source is both time consuming and prone to various numerical errors, it is convenient in studying the low frequency wave drift damping phenomenon to expand the Green function as a perturbation series in terms of the forward speed, retaining only those terms linear in U. Thus the alternative, and equivalent, source strength based forward speed integral equation

$$-\alpha\sigma = \int_{S_w} \sigma \frac{\partial G}{\partial n} ds + \frac{U^2}{g} \oint_{L_0} n_1 \sigma \frac{\partial G}{\partial n} dy - v_n, \qquad (7)$$

with ϕ recoverable from

$$\phi = \int_{S_w} \sigma G ds,$$

is reduced to the coupled integral equations

$$-\alpha\sigma_0 = \int_{S_w} \sigma_0 \frac{\partial G_0}{\partial n} ds - v_{n_0}$$

$$-\alpha\sigma_1 = \int_{S_w} \sigma_1 \frac{\partial G_0}{\partial n} ds - \int_{S_w} \sigma_0 \frac{\partial G_1}{\partial n} ds - v_{n_1}, \qquad (8)$$

with ϕ recoverable from $\phi_0 = \int_{S_w} \sigma_0 G_0 ds$ and

$$\phi_1 = \int_{S_w} \sigma_1 G_0 ds + \int_{S_w} \sigma_0 G_1 ds.$$

Here G_1 is a forward speed correction [7] derivable from the zero speed Green function G_0. In effect G is assumed to satisfy $G = G_0 + \tau G_1$ and σ satifies $\sigma = \sigma_0 + \tau\sigma_1$ where $\tau = U\omega_e/g$.

As the first stage of a more complex formulation, not explained here, we finally consider the Green Function Matching technique based on the linearised forward speed Green function method of Equation (6). The artificial outer integral equation formulation is now given by

$$\begin{aligned} -\alpha\phi' + \int_{S_\tau} \phi' \frac{\partial G}{\partial n} ds - 2i\frac{U\omega_e}{g} \oint_{L_\tau} G\phi' dy \\ + \frac{U^2}{g} \oint_{L_\tau} \left[\phi' \frac{\partial G}{\partial x} - G\frac{\partial \phi'}{\partial x}\right] dy = \int_{S_\tau} G \frac{\partial \phi'}{\partial n} ds \end{aligned}, \qquad (9)$$

where, as before, ϕ' is the outer domain solution and L_τ is the line of intersection of S_τ and S_f. The corresponding inner Rankine source integral equation formulation is given by

$$\begin{aligned} -\alpha\phi + \int_{S_w} \phi \frac{\partial G}{\partial n} ds + \int_{S_\tau} \left[\phi \frac{\partial G}{\partial n} - G\frac{\partial \phi}{\partial n}\right] ds \\ + \int_{S_f} \left[\phi \frac{\partial G}{\partial n} - \frac{1}{g}\left[\omega_e + iU\frac{\partial}{\partial x}\right]^2 \phi G\right] ds = \int_{S_w} G\, v_n ds \end{aligned} \qquad (10)$$

Since the purpose of this paper is to transmit the basic ideas of HOBE formulations the mathematical forms [8,9] of G for pulsating and translating pulsating sources for finite and infinite water depth are not specified here.

3. THE HIGHER ORDER BOUNDARY ELEMENT APPROACH

As already indicated the use of curved panels and higher order functional representations of the unknown velocity potential, or source strength, require interpolation functions within each element. Here 'serendity elements', in the terminology of finite elements [10], are used. In such elements the approximations used only depend upon the support of nodes on the boundary of the element. The interpolation functions or shape functions are simply polynomials in the variables u and v, say, which define a set of curvilinear coordinates over each element [1,11]. The order of approximation used to represent the geometry and the unknown variables need not be the same. Both quadratic and cubic representations over quadrilateral and triangular elements have been considered. The number of nodes per element are therefore 8 and 6, and 12 and 10 for the quadratic and cubic representations respectively. For plane boundary elements it is normal to have one node only at the element centroid.

If $\underline{r}\,(\xi,\eta,\varsigma)$ denotes the position vector of a generic point of an element then

$$\underline{r}(\xi,\eta,\varsigma) = \sum_{k=1}^{n} \underline{r}(\xi_k,\eta_k,\varsigma_k) N_k(u,v)$$

and (11)

$$\phi(\xi,\eta,\varsigma) = \sum_{k=1}^{m} \phi(\xi_k,\eta_k,\varsigma_k) M_k(u,v),$$

where n and m, as just indicated, depend on the degree of the representation of the element geometry and velocity potential respectively for the selected element geometry, and N_k and M_k are the shape functions evaluated at the k^{th} node of the element located at $(\xi_k, \eta_k, \varsigma_k)$. Thus (ξ, η, ς) represents the coordinates of a generic point on an element and $(\xi_k, \eta_k, \varsigma_k)$ denotes the specific points used to define the element representation. Otherwise we shall refer to the implicitly assumed right handed Cartesian reference system $O(x, y, z)$, with x forward in the direction of advance and z positive above the undisturbed free-surface. The area transformation for the surface integrals and the local unit normal vector on the element are expressible as

$$ds = J(u,v)du\ dv,$$

and (12)

$$\hat{n} = \frac{t_u \wedge t_v}{J(u,v)}$$

respectively, with the Jacobian and local element tangential vectors given by

$$J(u,v) = |\, t_u \wedge t_v \,|,$$

$$t_u = \sum_{k=1}^{m} \frac{\partial N_k}{\partial u} \underline{x}(\xi_k, \eta_k, \varsigma_k),$$

and (13)

$$t_v = \sum_{k=1}^{m} \frac{\partial N_k}{\partial v} \underline{x}(\xi_k, \eta_k, \varsigma_k).$$

Thus, the discretised form of the zero speed Green function formulation of Equation (1) may be expressed as

$$-\alpha\phi + \sum_{j=1}^{N}\sum_{k=1}^{m} \phi(q_k^j) \int_{S_j}\int M_k(u,v)\Big(n_\xi \frac{\partial G}{\partial \xi} + n_\varsigma \frac{\partial G}{\partial \varsigma} + n_\eta \frac{\partial G}{\partial \eta}\Big) J(u,v)du\ dv = \sum_{j=1}^{N} \int_{S_j}\int G v_n J(u,v)du\ dv \tag{14}$$

where N is the total number of elements used to model the wetted surface boundary S_w. We may also approximate normal derivatives of the velocity potential to the same degree m, thus

$$\frac{\partial \phi'}{\partial n} = \sum_{k=1}^{m} M_k(u,v) \frac{\partial \phi'(\xi_k, \eta_k, \varsigma_k)}{\partial n} \tag{15}$$

is used in the zero speed Green Function Matching technique formulation of Equation (5).

The solid angle α associated with the integral equation formulations must be interpreted with care. For example, for the corner point of a rectangular box form of S_r the solid angle is $\pi/2$ for the inner problem formulation and $7\pi/2$ for the outer problem formulation. Since α is the angle subtended at a point by a surface S then it only has the value 2π when S is smooth at the point of interest. Otherwise a scheme investigated by Hearn and Donati [11] is used. For nodal points on the intersection of the wetted surface, S_w, and the free surface, S_f, the solid angle definition must also take into account the contribution from the image part of the Green function. The consequence of not using the correct solid angle at the free-surface was previously demonstrated in the 2D HOBE paper[1].

For plane boundary elements analytic integration of the Rankine source and its derivative have been well established [12] for a long time. For curved elements there is no convenient corresponding analytic procedure. Therefore all integrations undertaken are numerical, using Gaussian product rules. However, when a field point is located on the element of integration, or very close to it, the Rankine part of the Green function G becomes singular or near singular. Fortunately using a local polar transformation on the element the singularity can be effectively eliminated [11].

For the different forward speed formulations, see Equations (6), (9) and (10), first and second order derivatives of the unknown potential are involved because of the forward speed effects. These quantities are obviously not known before the boundary value problem is solved. The advantage of the HOBE approach is that such derivatives may now be expressed in terms of the element shape functions and its derivatives. Thus it may be shown that

$$\underline{\Phi} \equiv \begin{bmatrix} \frac{\partial \phi}{\partial x} \\ \frac{\partial \phi}{\partial y} \\ \frac{\partial \phi}{\partial z} \end{bmatrix} = [T^{-1}] \begin{bmatrix} \frac{\partial \phi}{\partial u} \\ \frac{\partial \phi}{\partial v} \\ \frac{\partial \phi}{\partial n} \end{bmatrix} \equiv [T^{-1}]\underline{\Phi}'$$

where (16)

$$T = \begin{bmatrix} \frac{\partial x}{\partial u} & \frac{\partial y}{\partial u} & \frac{\partial z}{\partial u} \\ \frac{\partial x}{\partial v} & \frac{\partial y}{\partial v} & \frac{\partial z}{\partial v} \\ \frac{\partial x}{\partial n} & \frac{\partial y}{\partial n} & \frac{\partial z}{\partial n} \end{bmatrix}$$

and the elements of T and $\underline{\Phi}'$ can be readily evaluated by direct differentiation of the shape function relationships defined in Equation (11). The second order derivatives satify

$$\begin{bmatrix} \phi_{xx} & \phi_{xy} & \phi_{xz} \\ \phi_{yx} & \phi_{yy} & \phi_{yz} \\ \phi_{zx} & \phi_{zy} & \phi_{zz} \end{bmatrix} = [T^{-1}][S][T^{-1}]^t, \tag{17}$$

where the superscript t denotes matrix transpose. The matrix S is defined by

$$S = \begin{bmatrix} \phi_{uu} - D_{11} & \phi_{uv} - D_{12} & \phi_{un} - D_{13} \\ \phi_{uv} - D_{21} & \phi_{vv} - D_{22} & \phi_{vn} - D_{23} \\ \phi_{un} - D_{31} & \phi_{vn} - D_{32} & \phi_{nn} - D_{33} \end{bmatrix}$$

where (18)

$$D = \Big(\frac{\partial}{\partial u}[T]\underline{\Phi}, \frac{\partial}{\partial v}[T]\underline{\Phi}, \frac{\partial}{\partial n}[T]\underline{\Phi}\Big).$$

Since the polynomial shape functions are at least twice differentiable most of the quantities are deducible directly from the shape functions. The only quantity which cannot be evaluated directly from differentiation of the shape function is ϕ_{nn}. This we determine by appealing to Laplace's equation. The resulting transformation [2] is too complex to present here. The important point to note however is that it can be done, and may be expressed in terms of T, D and similarly defined quantities.

All the component elements of the S and D coefficients may be shown to satisfy the reciprocal relationships

$$D_{jk} = D_{kj}$$

and (19)

$$\phi_{ab} = \phi_{ba}$$

for $j,\ k\ =\ 1,\ 2\ \&\ 3$ and for ab equal to un, uv and vn.

In the implementation of the HOBE method geometric symmetry has been exploited. Thus symmetric and anti-symmetric potentials are solved separately. In the outer problem of the Green Function Matching method care must be exercised when determining the anti-symmetric solutions because, for port-starboard symmetry say, the row matrix for G becomes indentically zero when the field point is located on the plane of symmetry. Direct matrix solution is therefore not possible. This problem does not occur in the inner problem formulation because the diagonal of the influence matrix is determined from the normal derivative of G and this is never identically zero. This outer solution problem can be eliminated by either avoiding field points near the plane of symmetry or assigning the potential values to be zero on the plane of symmetry. The latter approach has the advantage of reducing the order of the associated influence function matrix, and makes conventional matrix inversion techniques applicable, once again. This fairly minor problem is a consequence of treating Equation (5), or (11), as Fredholm first kind rather than as a Fredholm second kind integral equation.

4. SECOND ORDER FORCE EVALUATION

The mean forward speed dependent second order forces and moments, determined from direct integration of the near-field pressures, are evaluated from

$$\begin{aligned}\overline{F}_m^{(2)} &= \frac{1}{4}\rho g\int_{L_w}|\zeta_a|^2\overline{N}dl - \frac{1}{4}\rho\int_{S_w}|\nabla\phi|^2\overline{n}ds \\ &+ \frac{1}{2}Re[\theta_{1a}^*\cdot F_a^{(1)}] - \frac{1}{2}\rho\omega_e\int_{S_w}Im[\delta_{1a}^*\cdot\nabla\phi]\overline{n}ds \\ &+ \frac{1}{2}\rho U\int_{S_w}Re[\delta_{1a}^*\cdot\nabla\phi_x]\overline{n}ds \\ &+ \frac{1}{2}\rho g A_w x_{cf}Re[\eta_4^*\eta_6]\hat{k}\end{aligned} \tag{20}$$

subject to

$$\begin{aligned}\overline{F}^{(1)} &= -\rho\int_{S_w}(\frac{\partial}{\partial t} - U\frac{\partial}{\partial x})\phi\overline{n}ds \\ &- \rho g(0,0,\overline{\eta}_3 A_w - \overline{\eta}_5 A_w x_{cf})\end{aligned}$$

and

$$\overline{N} = (n_1, n_2, n_3)/(n_1^2 + n_2^2)^{\frac{1}{2}}.$$

Here, $\overline{N}$, has been introduced to account for the slope of the wetted surface at the free-surface. The above expressions and notation of Hearn and Tong [5] differ slightly to the zero forward speed expressions presented by Standing et al [13] and Pinkster[14]. Clearly, the evaluation of higher order derivatives is as important in the evaluation of the second order forces as in the HOBE formulations. In particular the speed associated term $U\nabla\phi_x$ will require appropriate transformations analogous to that for ϕ_{xx}. These have been derived [2] and implemented.

5. HOBE APPLICATIONS

HOBEs were not developed primarily to provide alternative solution techniques for the various first order fluid-structure interaction problems presented. It was an interest in second order hydrodynamic quantities, and the known sensitivity to the prediction method employed, which provided the motivation for the reported research. The numerical results presented are therefore for the second order quantities of mean drift force, added resistance and low frequency wave drift damping. The barge and semi-submersible considered are those previously investigated by Pinkster[14]. The principal dimensions, radii of gyration and displacements for both structures are set out in Table I. The drift and added resistance forces are computed using the near-field pressure integration formula presented. The low frequency wave drift damping is evaluated using the Added Resistance Gradient (ARG) method [4,8,18].

Table I. Principal Structural Characteristics

Description	Barge	Semi-Submersible
L (m)	150.0	100.0
B (m)	50.0	76.0
T (m)	10.0	20.0
KG (m)	10.0	8.64
r_{xx} (m)	20.0	30.5
r_{yy} (m)	39.0	30.9
r_{zz} (m)	39.0	41.7
∇ (m^3)	73750.0	34470.0

Discretisation of structures for 3D methods is not so automated as for 2D methods because of the need to represent complex surfaces rather than 2D curves. The selection of the nodes and the boundary elements requires care if both geometry and hydrodynamic flow characteristics are to be properly modelled. The number of nodes used in the HOBE procedure is likely to be high in practice because of the quadratic or cubic nature of the representations selected. Thus even for the relatively simple geometric form of the selected offshore barge, using quadratic elements, the discretisation of the wetted surface, the free-surface and the radiation boundary consists of 46, 36 and 48 boundary elements respectively. This leads to 169, 135 and 153 nodal points for each indicated surface , with 33 and 25 of these nodal points located on the wetted surface waterline, L_o, and the radiation water line, L_r, respectively. Great care is therefore required in the data preparation. There is no room for complacency. The Pinkster semi-submersible has six columns. Each column has been discretised into two rows of just four facets. The pontoons are of rectangular transverse section. The total number of nodes used in this case is 487, with 186, 182 and 161 on the wetted surface of the semi-submersible, the free-surface and radiation boundary respectively. The plotted barge discretisation looks relatively trivial, even when it is not, so only the semi-submersible discretisation is presented in Figure 1.

The results presented in Figures 2 and 3 are the added resistance forces for the Pinkster barge in head (180°) and bow oblique (135°) waves in the absence of current at various forward speeds, U. These particular results were computed using the zero speed Green function formulation with strip-theory forward speed corrections applied. This approach is designated HOBEGRN. In the oblique wave condition the surge drift force has a distinct trough and peak, which is not exhibited in the head sea results. Because of this difference the resultant low frequency surge damping presented in Figure 4 is distinctly different for the two wave headings. The wave drift damping in the head sea condition is positive over the frequency range considered, whereas it becomes negative at non-dimensional frequencies above 3.2 for the oblique wave heading. The negative damping occurs at a frequency associated with a cross over of the different forward speed added resistance curves. The first order quantities have been compared with Pinker's predictions. The agreement was very good.

Figure 5 provides a comparison of the zero speed surge drift force for the semi-submersible subject to a head sea condition. The results presented include the Pinkster experimental mea-

surements, the constant-source plane-boundary element predictions of Hearn and Tong [16] and the new HOBEGRN based predictions. Figure 6 shows a similar comparison for the bow oblique wave (135°) heading. The agreement between the two sets of predictions in each case is good within the frequency range considered. The agreement with the experimental results is also encouraging.

Figures 7 and 8 present the added resistance curves for the semi-submersible for five different forward speeds for the same two wave headings. Unlike mono-hull structures, the added resistance force curves for the semi-submersible tend to cross over each other at different frequencies for different forward speeds. To appreciate the difference the interested reader could compare the semi-submersible characteristics with those of the various plane boundary element ship predictions reported previously [17]. In so doing one would immediately note that the lowest forward speed no longer necessarily gives the lowest added resistance in the case of the semi-submersible. Figure 9 provides the corresponding wave drift damping coefficients for the two wave headings. The damping values now oscillate about the zero level and both the relative phase and magnitude of the damping are quite distinct for the two wave headings.

6. CONCLUSIONS AND FINAL COMMENTS

In theory, the HOBE scheme should give more accurate predictions, but in practice this is difficult to justify without very elaborate discretisation convergence tests. Furthermore, it has been difficult to establish any relationship between the effects of varying frequency and forward speed upon the convergence of the predictions. However, the HOBE representation does provide some definite advantages over the constant-source plane-element method. In particular, the line integrals of the forward speed formulations are actually evaluated on the water line of the structure rather than at the centroid of the plane-elements nearest the water line. Similarly the derivatives of the potential are evaluated on the actual water line when evaluating the second order hydrodynamic quantities. This is because the HOBE scheme allows the line integral and the derivatives to be evaluated directly without resorting to numerical means.

The numerical results available (but not presented here) are sufficient to establish [2] that the Rankine source based singularity formulation of the inner problem, Equation (2) or (10), can be used as an effective solution technique for the water wave radiation and diffraction problems. The simplicity of the fundamental singularity allows the governing integrals to be evaluated efficiently and accurately. Furthermore, the frequency independent nature of the fundamental singularity also enables their integration to be undertaken once and then used in all subsequent calculations for different frequencies. The remaining computational task for each new frequency is thus reduced to the re-assembling of matrices and their solution without re-evaluation.

Although the existence and uniqueness of the solution of the outer problem in the Green Function Matching scheme has not been formally proved the numerical results generated to-date [2] indicate that such a scheme is stable and accurate within the practical frequency ranges considered. In the low frequency regime, the numerical results based on the Green Function Matching and the direct Green function methods are almost indistinguishable. At the higher frequencies either a finer mesh on the free-surface or a higher order representation of the sought unknown function is required to maintain the stability of the fundamental singularity distribution. The use of the fundamental singularity in the forward speed problem has not yet been fully explored.

In the zero speed problem, the Green Function Matching scheme has the advantage over the Sommerfeld scheme of being independent of the shape and the position of the radiation boundary. In practice this allows the radiation boundary to be placed very much closer to the body and thus reduces the size of the fluid domain involved in the computation. In contrast the validity of the Sommerfeld radiation condition of Equation (3) is governed by the appropriateness of the position of the radiation boundary S_r for the particular fluid-structure interaction problem being investigated.

The independence of the Green Function Matching scheme to the shape of the radiation boundary also enables one to select the most convenient geometry for efficient evaluation of the Green function. Once the outer problem is solved, the influence matrix defined by $G^{-1}[\frac{\partial G}{\partial n}]$ can be evaluated and stored. This matrix of coefficients is then usable for different geometric structures in the inner problem at the same frequency without re-evaluation. Therefore the outer problem in the Green Function Matching scheme is only solved once for each frequency. The computational effort incurred may thus be considered as an initial 'set-up cost' for all future analyses. However, the Green Function Matching technique appears to converge to a different solution at much higher frequencies. Further research is therefore required to establish whether,

(i) this technique simply does converge (correctly or otherwise) to a different limit, or

(ii) the procedure is providing distinctly different results which may be found to be justifiable through experimental observation.

The mathematical detail presented has been kept to a minimum. However, the presented detail should be sufficient to demonstrate the general applicability of the HOBE method to a number of quite distinct hydrodynamic analyses. Particular mathematical and computational difficulties and their solution have been highlighted. The formulation and solution of the integral equations is available in greater mathematical detail in references 11, 18 & 2. The numerical results presented show that the higher order representation of the geometry of the structure, and the distribution of the velocity potential over the structure, provides results consistent with (i) the constant source approximation associated with plane boundary element schemes and (ii) experimentally measured data for the semi-submersible. The barge and the semi-submersible results also demonstrate the sensitivity of the second order quantities to wave heading and forward speed. For some naval architects the geometries considered might be just too box-like in form and therefore a HOBE discretisation of a Series 60 ship of $C_B = 0.8$ is presented in Figure 10. This also illustrates that more complex shapes can be handled and shows how one might represent the free-surface. In fact this particular ship form has been investigated, using the HOBE approach, without and with a turret mooring opening located some 25% of its length from the FP [19]. A comparison of the predicted second order quantities again demonstrates great sensitivity.

The HOBE concept, in the opinion of the author, is both useful and applicable to many offshore related free-surface fluid-structure interaction problems. The use of the shape functions, well known in finite element methods, facilitates the solution of the most complex forms of the different open water integral equation formulations presented. In the course of time it will be demonstrated that the procedure is equally applicable in the analysis of the confined water problems considered in reference 3.

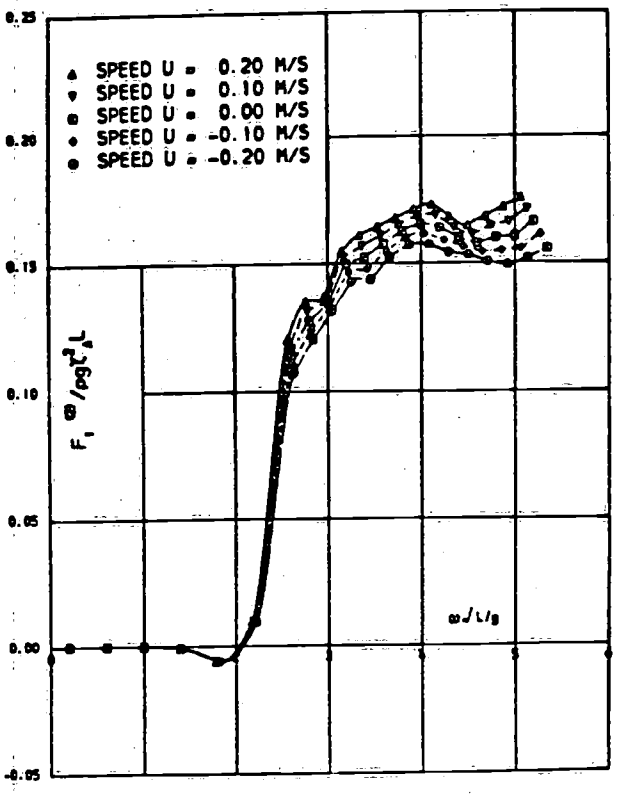

Figure 2. Added Resistance of Pinkster Barge in Head Seas.

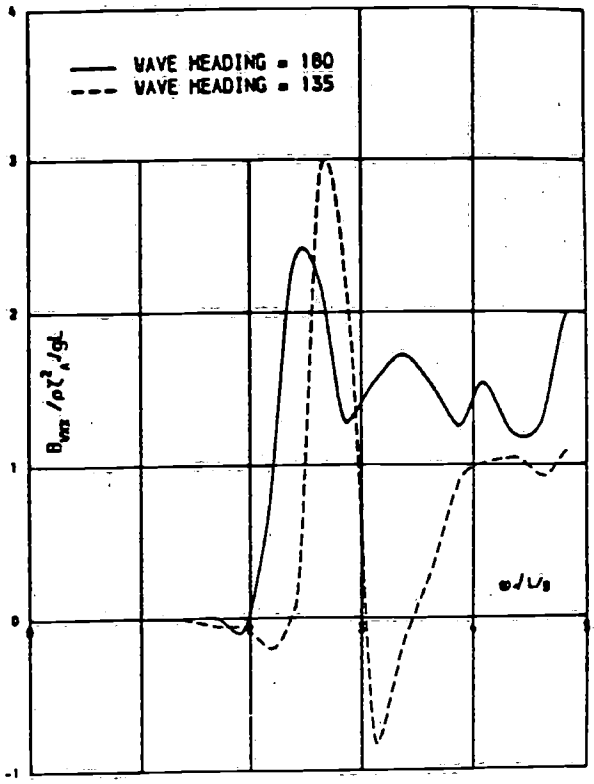

Figure 4. Surge Low Frequency Damping of Pinkster Barge.

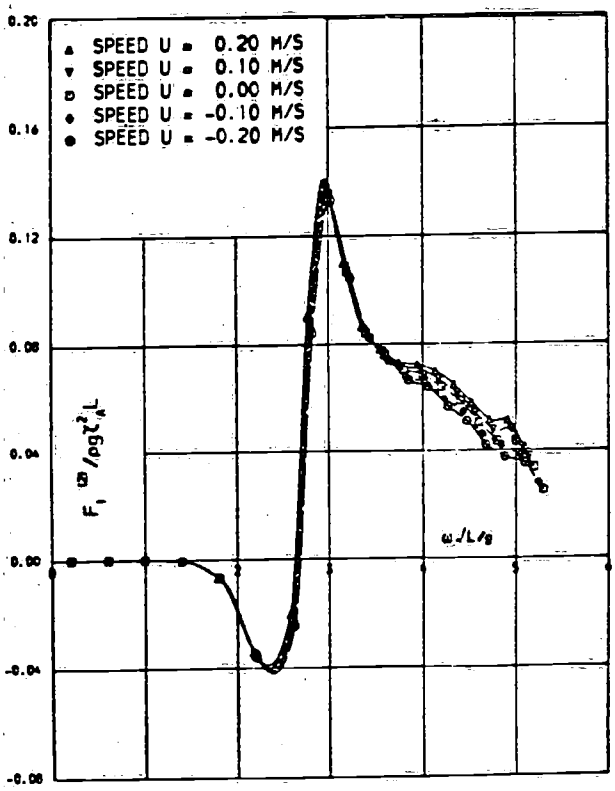

Figure 3. Added Resistance of Pinkster Barge in Bow Seas.

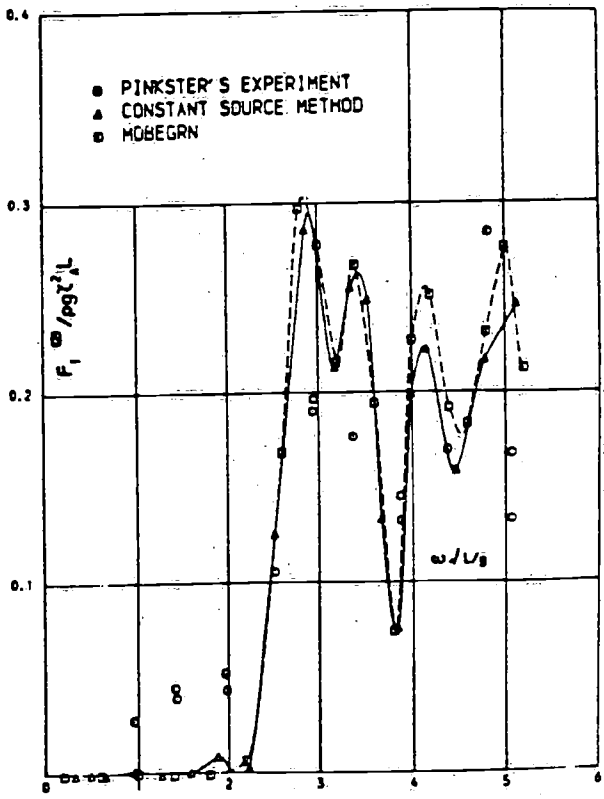

Figure 5. Head Sea Drift Force Predictions for Pinkster Semi-Submersible.

ACKNOWLEDGEMENTS

The research reported was made possible through the financial support of the Marine Technology Directorate of the Science and Engineering Research Council (SERC MTD Ltd.). The actual HOBE calculations reported were undertaken by Dr.S.M.Lau, the Research Associate for the project [3]. Miss Kathleen Heads' assistance with the typing of the paper, Mrs. Judith Hunter's assistance with the mathematical 'niceties' of TEX wordprocessing and Mrs. Jennifer Hearn's proof reading are gratefully acknowledged. Responsibility for the opinions expressed lies entirely with the author.

REFERENCES

1. Hearn, G.E. and Donati, E., "A New Fluid - Structure Interactin Analysis Based on Higher - Order Boundary Elements", Int. J. Numerical Methods in Fluids, Vol.8, 1988, p.199
2. Hearn, G.E. and Lau, S.M., SERC MTD Floating Production Systems Managed Programme, 1987-89, Final Contract Report, "Low Frequency Damping Predictions and Behaviour of Marine Structures in a Seaway", Dec. 1989.
3. Hearn, G.E. and Liou, S.Y., "Finite Depth and Tank Wall Effects Upon First And Second Order Forces", Proceedings of International Offshore Mechanics and Arctic Engineering (OMAE) Symposium, Vol.I, Part A, Feb. 1990, p.171.
4. Hearn, G.E. and Tong, K.C., "Evaluation of Low Frequency Wave Damping", Proceedings of 18th Offshore Technology Conference, Paper 5176, 1986.
5. Hearn, G.E., Tong, K.C. and Lau, S.M., "Sensitivity of Wave Drift Damping Coefficient Predictions to the Hydrodynamic Analysis Models used in the Added Resistance Gradient Method", Journal of Offshore Mechanics and Arctic Engineering, Vol.110, No.4, Nov. 1988, p.337.
6. Hearn, G.E. and Tong, K.C., "A Comparative Study of Experimentally and Theoretically Predicted Wave Drift Damping Coefficients", Proceedings of 21st Offshore Technology Conference, Paper 6136, 1989.
7. Huijsmans, R.H.M. and Hermans, A.J., "A Fast Algorithm for Computation of 3-D Ship Motions at Moderate Forward Speed", Proceedings of 4th International Conference on Numerical Ship Hydrodynamics, Washington, USA, Sept. 1985.
8. Wehausen, J.V. and Laitone, E.V., "Surface Waves", Handbuch der Physik, Vol.IX, 1960, p.446.
9. Lau, S.M., "3-D Hydrodynamic Analysis of First and Second Order Forces on Free Floating Structures with Forward Speed", Ph.D. Thesis, Department of Naval Architecture and Shipbuilding, University of Newcastle upon Tyne, 1987.
10. Zienkiewicz, O.C., "The Finite Element Method", M^c Graw Hill, 1977.
11. Hearn, G.E. and Donati, E., SERC MTD Compliant Systems Cohesive Programme, 1983-85, Final Contract Report, "Higher Order Boundary Elements", 1985.
12. Hess, J.L. and Smith, A.M.O., "Calculation of Potential Flow about Arbitrary Bodies", Progress in Aeronautical Sciences, Vol.8, 1967, p.1.
13. Standing, R.G., Dacunha, N.M.C. and Matten, R.B., "Mean Wave Drift Forces: Theory and Experiment", National Maritime Institute (NMI), Report R124, 1981.
14. Pinkster, J.A., "Low Frequency Second Order Wave Exciting Forces on Floating Structures", Netherlands Ship Model Basin Report 650, 1980.
15. Wichers, J.E.W. and van Sluijs, M.F., "The Influence of Waves on the Low Frequency Hydrodynamic Coefficients of Moored Vessels", Proceedings of 11th Offshore Technology Conference, Paper 3625, 1979.
16. Hearn, G.E. and Tong, K.C., SERC MTD Compliant Systems Managed Programme, 1985-87, Final Contract Report, "Second Order Fluid Damping", Sept. 1987.
17. Hearn, G.E., Tong, K.C. and Lau, S.M., "Hydrodynamic Models and Their Influence on Added Resistance Predictions", Proceedings of Practical Design of Ships and Mobile Units, Vol.1, 1987, p.302.
18. Hearn, G.E., "Using Mathematics to Simplify Free Surface Structure Interaction Analyses", International Conference on Computational Methods in Flow Analysis, Okayama, Japan, Sept. 1988.
19. Hearn, G.E., "Low Frequency Damping: The Development of its Theoretical Prediction", IUTAM Symposium on Dynamics of Marine Vehicles and Structures in Waves, Prof. R.E.D. Bishop Memorial Symposium, Brunel University, June 1990.

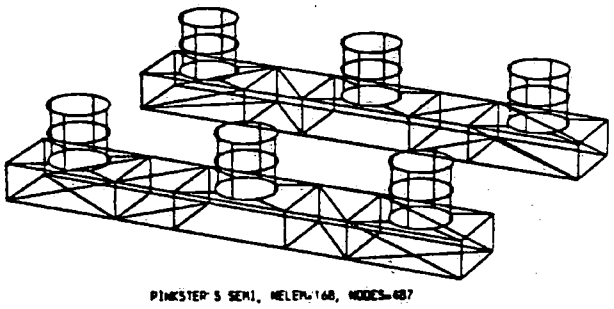

Figure 1. H.O.B.E Discretisation of Pinkster Semi - Submersible.

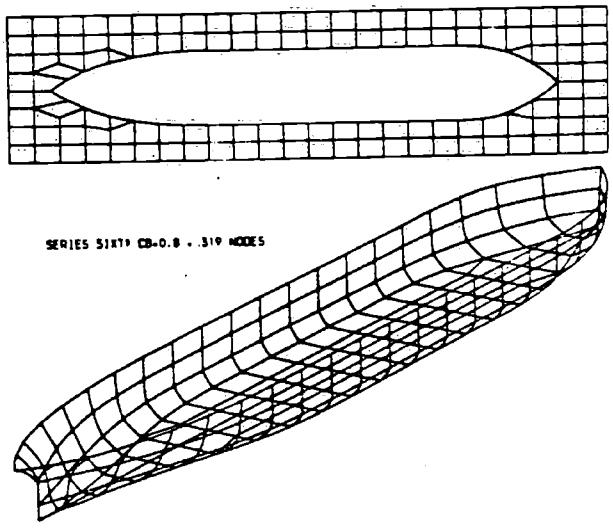

Figure 10. Series 60 H.O.B.E Discretisation.

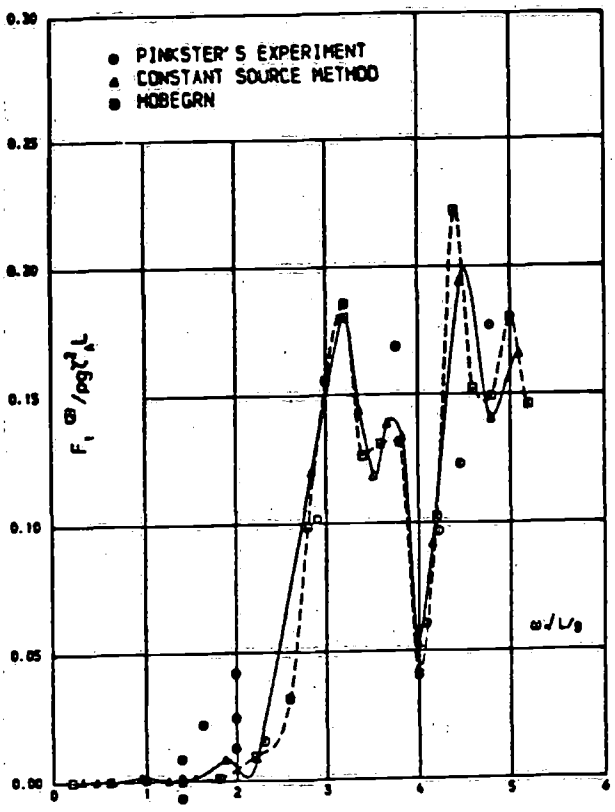

Figure 6. Bow Sea Drift Force Predictions for Pinkster Semi-Submersible.

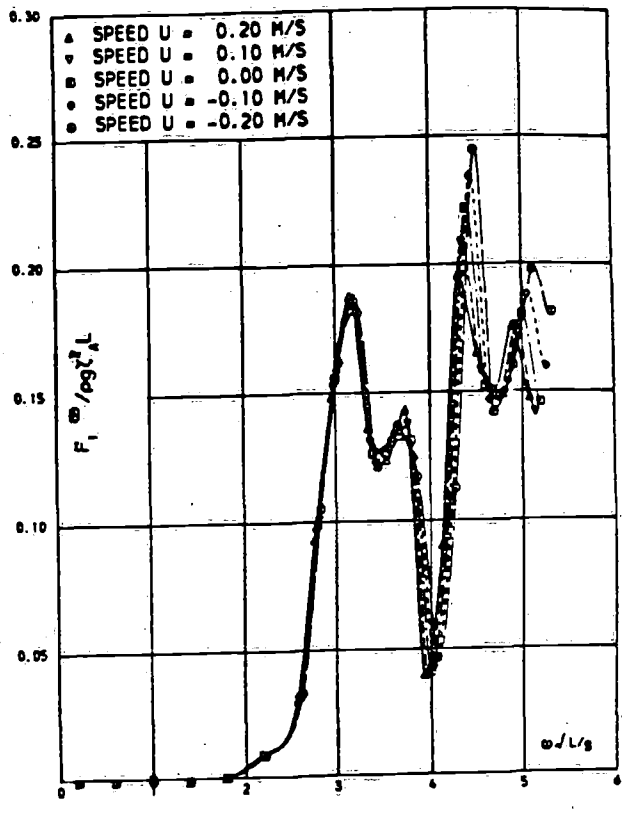

Figure 8. Added Resistance of Pinkster Semi-Submersible in Bow Seas.

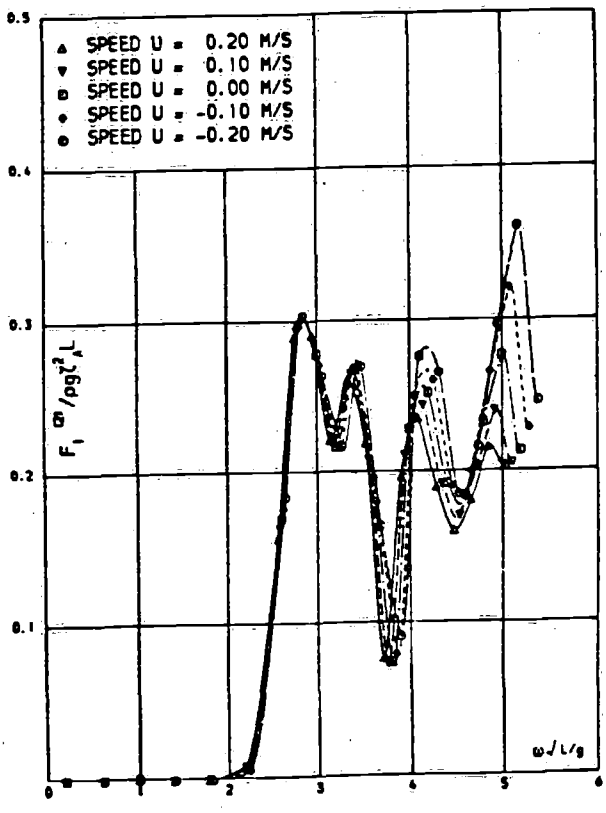

Figure 7. Added Resistance of Pinkster Semi-Submersible in Head Seas.

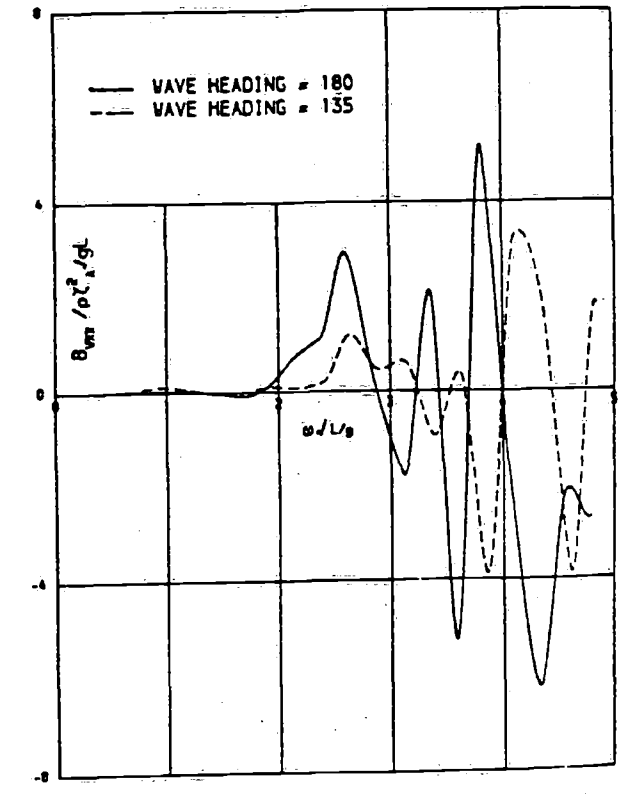

Figure 9. Surge Low Frequency Damping of Pinkster Semi-Submersible.